DOI: 10.1111/tgis.12797

RESEARCH ARTICLE

Transactions in GIS WILEY

Locating and categorizing causes of discomfort during transport of patients to medical facilities

Aleksandar Peulić[1] | Miodrag Peulić[2,3] | Željko Jovanović[4] | Miloš Joković[5,6] | Sanja Stojković[1] | Nemanja Vagić[1]

[1]Faculty of Geography, University of Belgrade, Belgrade, Serbia

[2]Faculty of Medical Sciences, University of Kragujevac, Kragujevac, Serbia

[3]Clinical Centre Kragujevac, Kragujevac, Serbia

[4]Faculty of Technical Science Cacak, University of Kragujevac, Cacak, Serbia

[5]Faculty of Medicine, University of Belgrade, Belgrade, Serbia

[6]Clinic for Neurosurgery, Clinical Centre of Serbia, Belgrade, Serbia

Correspondence
Nemanja Vagić, Faculty of Geography, University of Belgrade, 3/3 Studentski trg St, 11000 Belgrade, Serbia.
Email: nemanja.vagic@gef.bg.ac.rs

Abstract

This article presents geographic information system usage in transportation management for comfort calculations, analysing vehicle vibration data measured during patient transportation. The main goal of this article is to develop a methodology for automatic discomfort cause recognition (DCR) that may be tested under real life conditions. We analysed differences between uncomfortable locations detected by passengers during patient transportation (according to their subjective opinions) and uncomfortable locations detected by the measurement system. The measuring system is based on the three-axis accelerometer which is used to determine road comfort values for specific locations gathered by a GPS module. The results obtained were compared with data collected by passengers. During driving, when they experienced discomfort, passengers marked locations in near real time using the GIS. The data thus obtained were analysed with the data obtained by DCR. For the first time, the application of GIS provides analytical tools to create spatial data and define spatial data relations that determine comfort. Testing under real conditions, involving three separate cases, shows a high degree of correlation between the results. The proposed system allows dynamic comfort threshold criteria management and provides a visual representation of summarized tabular data.

1 | INTRODUCTION

Transport represents the first basic condition for the normal development of economic and social life. One of the most important underlying requirements for transport is good-quality road traffic conditions for the widespread and safe use of vehicles all over the world. Road safety is a complex system that involves drivers, vehicles, and roads. This means that improvements to road safety should address drivers' behaviour, the technical characteristics of the vehicles, and the condition of the roads. On most roads, bumps greatly affect traffic movement and control speed to ensure safety. Information about road conditions is highly desirable to allow the traffic to flow safely and comfortably within permissible speed limits. Passenger comfort is one of the most significant concerns. Even though ride comfort is a subjective experience for the driver and passengers travelling in a vehicle, noise, temperature, road conditions, and vehicle dynamics certainly influence ride comfort. An understanding of such factors is especially important in the case of patient transportation, as patients are passengers with health problems; ride comfort can have a greater influence on one's condition, which may already be precarious. Gray, Bush, and Whiteley (2004) divided the transportation of patients into primary transport (the transfer of patients from the site of illness or injury to the first hospital contact) and secondary transport (the transfer of the patient from one hospital to another for continuing clinical care).

All road authorities try to maintain the quality of roads within their jurisdiction, particularly with respect to the vibrations induced in the vehicles by road roughness. ISO 2631 (International Organization for Standardization [ISO], 1997) defines criteria that evaluate human whole-body vibration experienced by passengers during a ride, starting from the first instance of vertical acceleration recorded in the vehicle. ISO standards also establish vibration limits to reduce discomfort and maintain health and safety during various activities. “Comfort” is a term that has no strict definition; therefore, it is difficult to accurately measure and display. Factors that affect passenger comfort while driving include seat vibration, vibration of the hands and feet, acoustic vibration (noise), seat design, temperature, humidity, air pressure, and the distance between seats. Of all factors, research has shown that vibration levels (i.e., vibro-comfort) have the greatest impact on comfort. To overcome problems associated with tracking multiple frequencies at the same time and to simplify the tracking of results, a method of absorbed power has been developed. It suggests that vibro-comfort is proportional to the amount of vibration the human body absorbs. This yields only one value commensurate with vibro-comfort. Absorbed power is calculated as the sum of mechanical forces on each contact with the vehicle. Mechanical strength is calculated as the product of force and speed. Measurements of vibro-comfort thus far have predominantly been based on the sensitivity of the human body to vibrations of different frequencies. The generally accepted view is that vibro-comfort is directly proportional to the acceleration acting on passengers while the vehicle is in motion. This is why most previous studies have focused on measuring the sensitivity of the human body to the acceleration of different frequencies, and can be found in the literatures of inertial navigation systems (British Standards Institution [BSI], 1987; ISO, 1997), robotics, the automotive industry, and the measurement of human body kinematics (Yangi, 2007). Only the value of acceleration is needed to measure vibro-comfort. The required value of speed is obtained using integrals. To get the value of mechanical force, weighting functions are defined that depend on the mechanical properties of the human body.

Comfort research papers have previously addressed various techniques to determine passengers' comfort during rides, and some of them specifically deal with patient transport (Jovanović, Blagojević, Janković, & Peulić, 2019; Wheble, 1987). Suspension, tyres, drivers’ seats, and road types were tested for their influence on the comfort of passengers with lumbar disc herniation during a drive (Battié et al., 2002; Gruevski, Holmes, Gooyers, Dickerson, & Callaghan, 2016). The comfort values determined from these studies were based on real driving calculations as well as simulations. Yangi (2007) deal with the commonly used simulation software and corresponding models. Oijer and Edlund (2003, 2004) present a method which makes it possible to predict the durability of a vehicle in real operation, and they have also explained vehicle durability and driver comfort in relation to road obstacles. Several researchers have specifically designed algorithms to detect road roughness (Cuadrado, Dopico,

Perez, & Pastorino, 2012; Xiandong, Zhidang, & Feng, 2003). Cuadrado et al. (2012) were involved in a research project that aimed to develop automotive real-time observations based on detailed nonlinear multibody models and the extended Kalman filter. Simulation models have been created (Yangi, 2007), and tests to estimate comfort have been performed on many subjects and road surface types (Schmidt & Diedrich, 2007). Ride comfort is very important in certain parts of the industry, so there is a lot of work to be done to make specific improvements to industrial and transport vehicles such as trains and dump trucks (Cleon & Laurkis, 1996; Wang, Qian, Tang, Wen, & Chen, 2000; Zhang, 2018). Some researchers have studied the impact of tyre and suspension quality (Fenchea & Boltosi, 2006; Jianmin & Qingmei, 2009; Junoh et al., 2011; Strahman, Dueker, & Kimpel, 2000), while others (Eriksson et al., 2008; Mohan, Padmanabhan, & Ramjee, 2008) have evaluated road surfaces. Eriksson et al. (2008) investigate an application of mobile sensing: detecting and reporting the surface conditions of roads using a collection of sensor-equipped vehicles. Paulraj, Yaacob, and Andrew (2010) propose a vehicle comfort level indication to detect the comfort level in cars using an artificial neural network. Wu et al. (2007) show how neural networks can be used in longitudinal vehicle guidance for comfort adjustment. Tan and Park (2005) present an accelerometer-based internal navigation system.

There are studies about comfort detection but there are no studies about discomfort cause recognition (DCR), which is the main topic of this article. Different sources of discomfort produce different acceleration values (road bumps, potholes, acceleration or braking, skidding). In this article acceleration data are analysed within a GIS environment to locate and categorize causes of discomfort.

Since the spatial locations of causes of road discomfort are important, GIS usage is recommended. The main benefits of using GIS are: (1) efficient management of spatial and temporal data; (2) effective visualization, highlighting areas of concern; and (3) improved efficiency in detecting discomfort locations.

According to Lee and Kwan (2018), due to advances in tracking technology, a large quantity of movement data has been collected and analysed in various research domains. Geographic information systems provide complex data analytical tools. Acceleration data can be analysed in relation to detected sources of discomfort and plotted accordingly. GIS can also be used to compare discomfort locations automatically identified by the system with those identified subjectively by human participants in the study. Although Li, Goldberg, Chu, and Ma (2019) state that in-vehicle sensing platforms are typically very costly and only available commercially, inertial measurement units and lightweight sensors that are used for orientation estimation in numerous applications are inexpensive. Such sensors can therefore be placed in several different locations in the vehicle (e.g., in the seat or stretcher) to obtain more accurate measurements.

The main aim of this article is to develop a methodology for automatically recognizing sources of discomfort on road networks, and testing this methodology in real-life conditions. Three tests are presented: the first test is an example of primary transport of a patient, from the accident site to a hospital; the second is an example of secondary transport from one hospital to another through an urban centre; and the third is also an example of secondary transport, evaluating a section of road through a rural area. Passengers used a GIS to provide real-time explicit feedback on the locations and levels of discomfort. The GIS was also used to visualize the results and compare the system-generated locations and levels of discomfort with those identified by the passengers. The tests showed a high degree of correlation between the automatic and manually derived results, hence the method shows potential for agencies with responsibility for road management and maintenance, in addition to bus, taxi and ambulance transport management, but also for users who just want to travel with minimum discomfort.

2 | METHODS

In this study, an ISO standard algorithm is modified to provide information about discomfort causes. The ISO standard defines calculation of root-mean-square (RMS) acceleration on vertical *Z* accelerations. With a one-axis accelerometer it is possible to calculate comfort, but it is not possible to detect various types of discomfort, so a

three-axis accelerometer was used for comfort detection. This detects the difference between RMS caused by vibrations and RMS caused by inclination. The ISO standard is good for checking comfort in a controlled environment, but in real-life vehicle driving, unexpected situations are very common.

Comfort is directly proportional to the acceleration that passengers can feel during the ride. Current standard methods include ISO 2631-1 (ISO, 1997) and British Standard 6841:1987 (BSI, 1987). Both standards assume that the magnitude of acceleration, frequency spectrum, and duration represent the principal exposure variables that account for potential harmful effects. The acceleration measured at one or more of the points of entry of vibration to the body is used to quantify the magnitude of vibration. Methods based on acceleration are fast, conceptually simple, and technically hassle-free since acceleration is the quantity directly measured by detectors.

ISO 2631 depends for calculating RMS acceleration on vertical *Z* accelerations. RMS acceleration values on the user's body (a_{iRMS}) are given by:

$$a_{zRMS} = \sqrt{\frac{1}{n}\left(a_{z1}^2 + a_{z2}^2 + \cdots + a_{zn}^2\right)} \tag{1}$$

where a_{zi} is the *i*th *Z*-axis sample acceleration. Obtained a_{zRMS} values must be multiplied by the weighting factor values W_K (because the human body has different vibration sensitivities, depending on the characteristic frequencies of vibrations) corresponding to these frequency bands. In the end, it is possible to determine the *vertical weighted RMS acceleration*, a_{WZ}. This is given by:

$$a_{WZ} = \sqrt{\sum (w_{k,i} \cdot a_{izRMS})^2} \tag{2}$$

This standard generates a single value in terms of acceleration due to gravity (G), which can be categorized in relation to comfort levels as shown in Table 1.

The main problem is the determination of the weighting factor. However, at lower intensity levels, the body finds all frequencies equally objectionable. Under normal driving conditions, vibration levels are lower and all frequency weightings are similar. The most commonly used weights are described in ISO 2631 and are used in the calculation of vibration dose values.

2.1 | Measuring system

The measuring system employed in this study uses accelerometer values to determine the road comfort value for a specific location defined by GPS position. The control unit (CPU) reads the measured acceleration values from the accelerometer sensor and the GPS coordinates of the system's current position from the GPS module. Processed

TABLE 1 Comfort levels related to a_{WZ} threshold values

Intervals of a_{WZ} values [G]	Comfort level
<0.315	Not uncomfortable
0.315–0.63	A little uncomfortable
0.63–0.8	Fairly uncomfortable
0.8–1.25	Uncomfortable
1.25–2.5	Very uncomfortable
>2.5	Extremely uncomfortable

Source: ISO (1997).

data are forwarded to a laptop computer via a USB connection. The data are then processed and formatted in KML file format, which is an XML file suitable for viewing in Google Earth (Open Geospatial Consortium, 2015).

The accelerometer is an ST Microsystems three-axis, 2g/6g inertial sensor LIS3L02AQ. For each axis, the maximum sample rate is 160 Hz. The central microprocessor is an 180 MHz AT91RM9200 made by ATMEL Corp., which is more than enough for running this application. A GM682-GPS module was also used. All signals were sampled at 100 Hz. The accelerometer used for comfort detection collects data at a minimum rate of 25 samples per second; however, system outputs were generated every 10 s taking into account all collected samples in a period of 10 s.

2.2 | Inclination compensation on measuring system—Equilibrium position calculation

The system must detect the difference between RMS caused by vibrations and RMS caused by inclination. Gravity has a great influence on accelerometer axis values.

Figure 1 shows driving uphill and downhill on a good-quality road. At first, the car was driven on an even surface, then uphill, then on an even surface again, then downhill, and on an even surface again (Figure 1a). The *X*-axis was insensitive (Figure 1c), the *Y*-axis was slightly sensitive (Figure 1d) but the *Z*-axis was very sensitive (Figure 1e) to this kind of driving. There are no acceleration peaks caused by an uneven surface. The presented values are simply caused by road inclination. This is reflected in the RMS value presented in (Figure 1f). Since the RMS value is calculated in 10 s time intervals, it is presented as a flat horizontal line. The detected value of 0.54G could be categorized as little uncomfortable (Table 1).

The compensation of gravity influence has to be done on the measuring system so the difference between RMS caused by vibrations and inclination can be detected. The average axis acceleration values and the differences between maximum and minimum values (Δx, Δy, Δz) for every axis are calculated in intervals of 1 s. The RMS caused by inclination is detected when the axis values are high but with no high acceleration values differences ($\Delta < 0.3$), thus it is not included in discomfort calculation. This functionality could be used for detection of vehicle turning during collisions. Vehicle turning is detected if Δx, Δy, and Δz are less than 0.3 and *X*, *Y* or *Z* values are not in logical value range relative to their position in a vehicle. Discomfort is detected if Δx, Δy, or Δz are greater than 0.3, even on inclined roads. In such cases, average axis values are used for RMS calculation.

2.3 | DCR algorithm—RMS with acceleration peak detection

It is possible to calculate comfort with a one-axis accelerometer; however, it is impossible to detect various types of discomfort. This is the main reason why a three-axis accelerometer is used for detection of discomfort. It collects data at a rate of at least 25 samples per second. Every sample contains *X*, *Y*, and *Z* accelerometer values (a_x, a_y, a_z) and accelerometer intensity, a, is calculated as:

$$a = \sqrt{a_x^2 + a_y^2 + a_z^2} \tag{3}$$

This algorithm modification allows detection of various types of isolated discomfort causes thanks to a three-axis accelerometer placed in a vehicle, oriented vertically by the *Y*-axis, so its value needs to be compensated for the influence of gravity. Axis influence when turning left or right, hitting a pothole or bump in the road, and sudden acceleration or braking is shown in Figure 2.

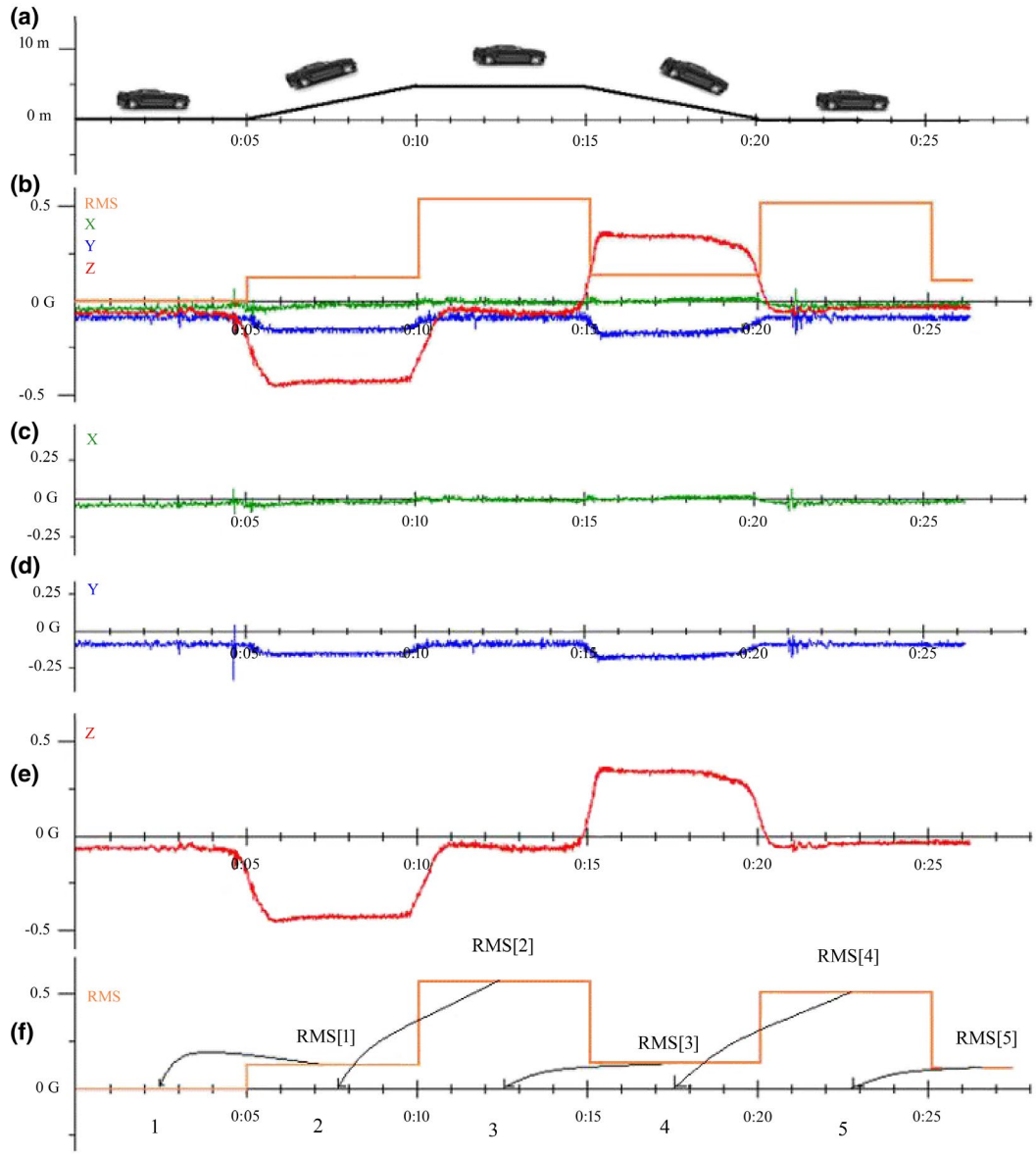

FIGURE 1 Uphill and downhill driving: (a) car motion; (b) all signals; (c) *X*-axis; (d) *Y*-axis; (e) *Z*-axis; and (f) RMS value

As Zhao and Stefanakis (2018) pointed out, the accelerometer measures the vehicle's acceleration in a three-axis frame, which can effectively capture the "jerk energy." The *X*-axis is sensitive to left and right turns. The *Y*-axis is sensitive to vertical jolts (potholes, bumps). The *Z*-axis is sensitive to sudden accelerations and deceleration. This is the main idea of this article: to analyse axis values in GIS software if discomfort is detected.

Some axes are more sensitive to some types of discomfort (Figure 2) but every axis detects some acceleration. As previously mentioned, beside the RMS calculation defined in ISO 2631, accelerometer threshold values (a_{peak}) detected in standard 10 s time intervals were also calculated. The ISO standard is good for checking comfort in a controlled environment. In real-life vehicle driving, unexpected situations, such as collisions, sudden braking, or sharp turns, are very common. These have a great influence on comfort, so the ISO standard algorithm is modified

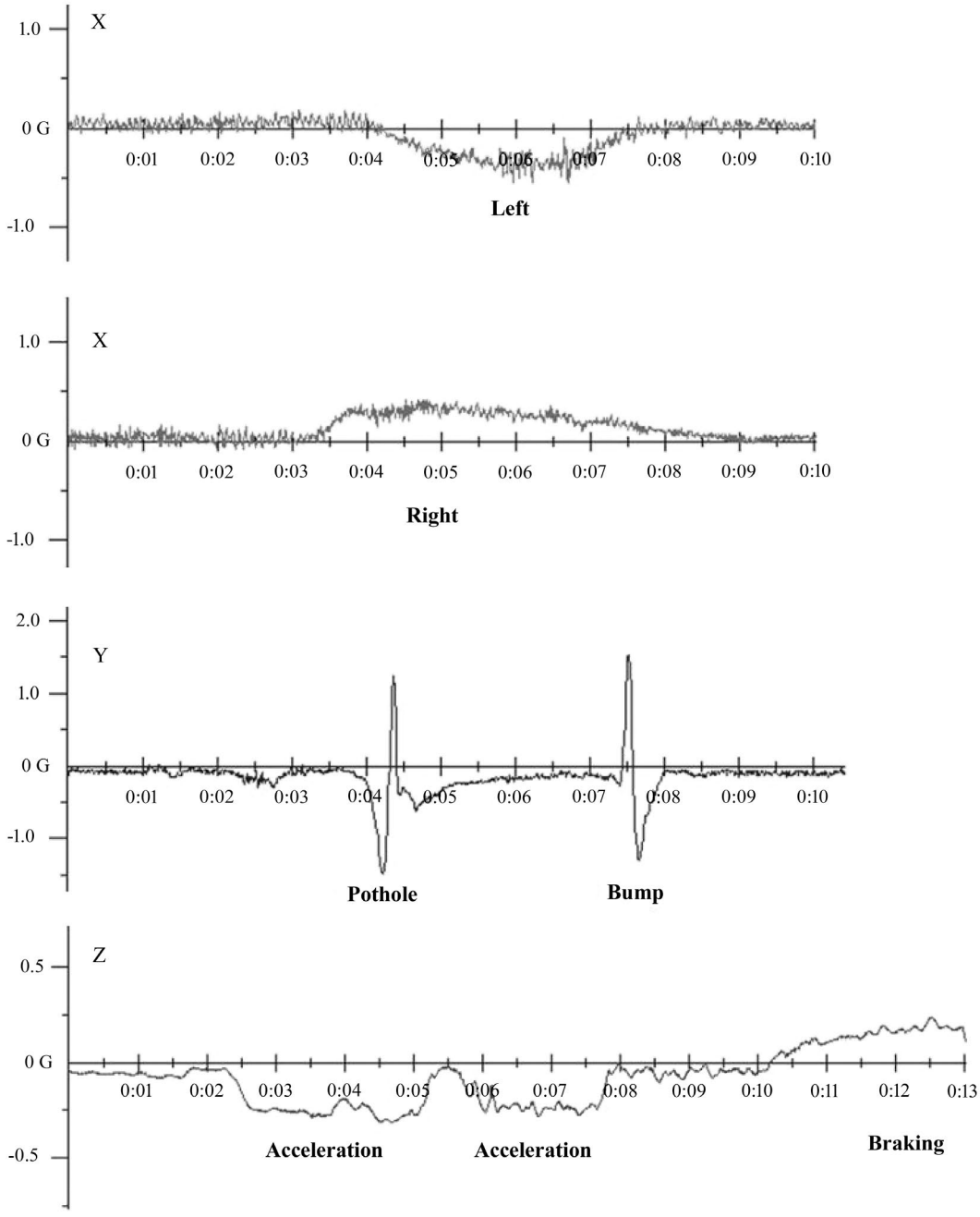

FIGURE 2 The appearance of accelerometer axis in different types of movement

to calculate an a_{peak} if uncomforted RMS is detected in the standard time interval. The RMS threshold value was initially set to 0.8G according to Table 1 and confirmed by GIS software analysis which is explained later in this article.

To detect discomfort type, it is necessary to analyse the highest acceleration value (a_{peak}) calculated by Equation 3 in detected discomfort. The causes of discomfort (Table 2) could be categorized based on *X*, *Y*, and *Z*-axis impact in a_{peak} and axis sensitivity (Figure 2).

TABLE 2 Discomfort cause types marker colour

Axis	Value sign	Recognized cause	Marker colour
X	+	Sharp turn right (drift)	Dark green
	–	Sharp turn left (drift)	Light green
Y	+	Road bump	Dark red
	–	Road pothole	Light red
Z	+	Intensive breaking (front hit)	Dark blue
	–	Intensive acceleration (hit from behind)	Light blue

By observing Figure 2 it is easy to detect activity by *X*- and *Z*- axis, but the problem is in the *Y*-axis since a road bump and a pothole create similar charts. This happens because the pothole creates high positive acceleration values as a consequence of hitting the pothole edge. This problem is solved by analysing the *Y*-value. The pothole is detected if it is initially a negative sign. A bump is detected if it is initially positive. *Z*-axis discomforts, "hit from the front" and "hit from behind," are included in the algorithm since they could be used in discomforts caused by collision situations. Three-axis acceleration values when impact occurs are shown in Figure 3.

Before impact, all axes oscillate slightly around 0 thanks to equilibrium position calculations. When an impact occurs, the vehicle and the accelerometer values oscillate until they calm down. This means that one impact could produce several values greater than a threshold value, which, however, does not mean that there were several impacts.

As shown in Figure 3a, when impact occurs, the acceleration intensity increases and a threshold value is achieved. This first acceleration intensity value higher than a threshold is important since it identifies the location of the cause of discomfort. All values except a_{peak} need to be rejected. This is done in real time within the measuring system. When the first value above the threshold ($|a_i| > a_{threshold}$ and $|a_{i-1}| < a_{threshold}$) is detected, the system calculates a_{peak} values in 1 s intervals. During this time the oscillations subside. Four peaks greater than a threshold value are detected (Figure 3) but are rejected.

2.4 | System testing in real-life conditions

The algorithm was tested in real-life by driving through the streets of Čačak, Serbia. Three independent tests were conducted (Figure 4). The first test was conducted on a 1.84 km long route which connects the city centre to the nearest hospital (route I). The measurements were made in May 2019. The passenger was a man, about 60 years old, without significant physical problems. The second test covered a 4.30 km long route through streets in the city centre from the hospital to the capital Belgrade with a higher-level health centre (route II). The measurements were made in August 2020. The passenger was a man, about 20 years old, with no major health problems. The third test was conducted in the rural areas of the municipality of Čačak in September 2020, on a 4.07 km road section that also forms part of the route towards the higher-level health centre in Belgrade (route III). The passenger was a 40-year-old woman with spinal problems.

The measurement system could be fixed in several places in the vehicle. Results presented in this article were collected with the measurement system fixed to the windscreen.

Passengers in the vehicle during the tests had to subjectively record discomfort in near real time by placing markers on images within the GIS. The supporting orthophotos (GUP Grada Čačka, 2019) had 30 cm precision, providing a high level of precision for mapping the location and severity of discomfort in real time.

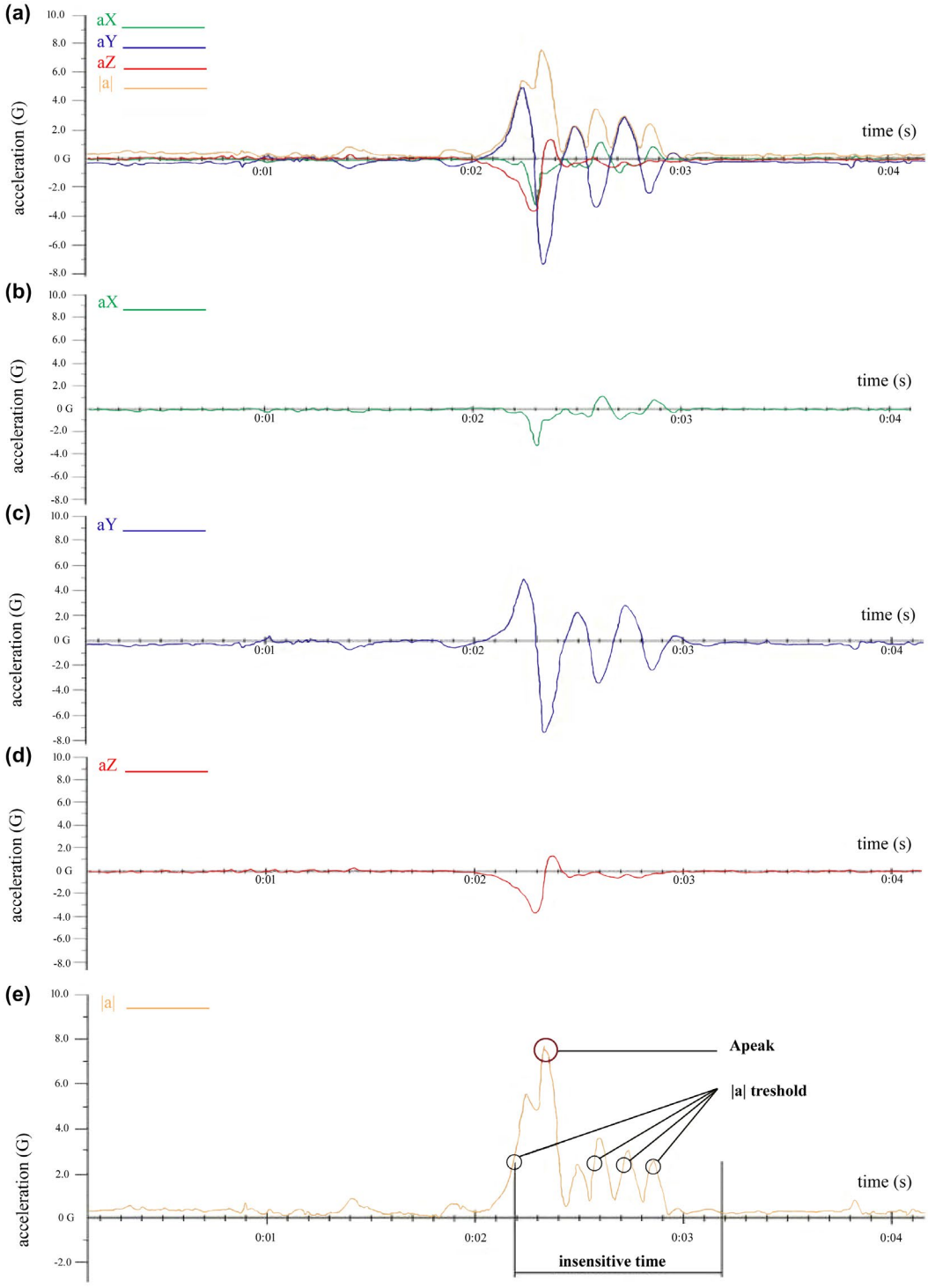

FIGURE 3 Acceleration oscillations in detected impact (zoom 2× in vertical values): (a) *X*-, *Y*-, *Z*-, and |*a*|-axis; (b) *X*-axis; (c) *Y*-axis; (d) *Z*-axis; and (e) |*a*|-axis

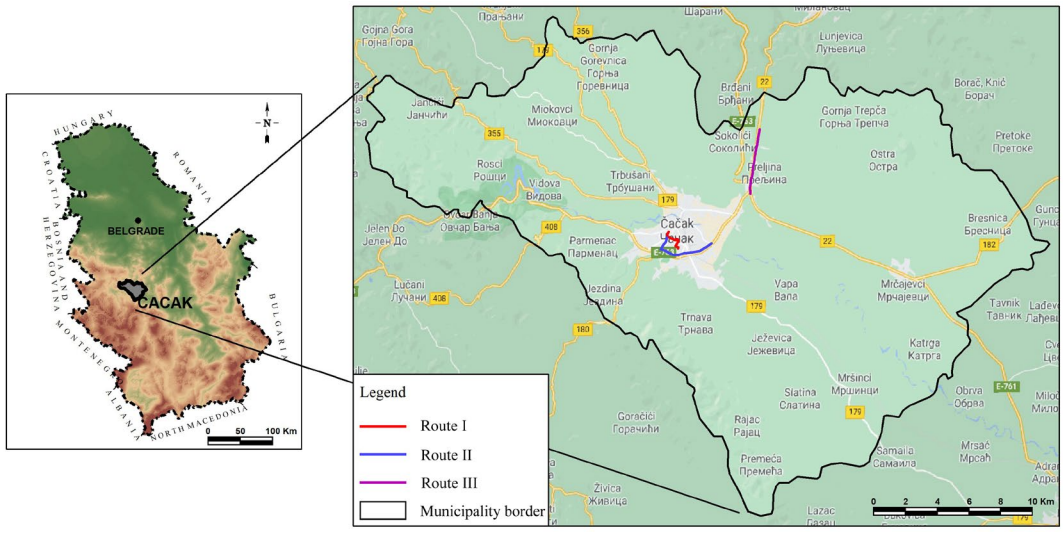

FIGURE 4 The geographic position of the study area and routes used to test the system. *Source*: https://www.google.rs/maps/

3 | RESULTS AND DISCUSSION

As previously mentioned, according to ISO 2361 and Table 1, discomfort is detected when RMS exceeds 0.8G. To confirm use of this threshold within the measurement system, the following tasks were completed:

- The measuring system was installed in a vehicle and the RMS threshold value was set to 0.5G. This threshold value was determined empirically based on repeat measurements and expert opinion. The lower value was set for detailed analysis and RMS value confirmation in practice. Measurements were taken while driving along three routes and results are presented in Figures 5a, 6a, and 7a.
- During driving, passengers marked locations on the GIS when they detected discomfort. Marker colours are chosen according to the discomfort types listed in Table 2. The results are shown in Figures 5b, 6b, and 7b.

During system testing on route I, as shown in Figure 5b, the passenger marked nine discomfort locations based on his subjective opinion. At the same time the measuring system detected 23 locations shown in Figure 5a. This is because the RMS threshold was set to 0.5G, not 0.8G. Marker counts by colour and RMS value for all three routes are shown in Table 3. It is important to note that all nine locations marked subjectively by the passenger were detected objectively by the system, that is, they share same geographic position.

The sum of dark red and blue markers (representing RMS > 0.8G) is 8. This means that system detected one discomfort location fewer than the passenger. Comparing the markers from both figures, marker no. 8 in Figure 5b (blue) is marked in red on Figure 5a (marker no. 22). This means that detected RMS is lower than 0.8G and that the RMS threshold values were not exceeded. A total of 23 locations were detected by the system overall, only four of which exceeded 1.2G.

During system testing on the route II, as shown in Figure 6b, the passenger marked seven discomfort locations. The measuring system detected 31 locations for the same route (Figure 6a). As in the case of route I, this is because the RMS threshold value was set to 0.5G instead of 0.8G. However, in this case, the sum of dark red and blue markers is seven (Table 3), which is in line with the subjective opinion of the passenger. Also, as in the case of route I, the geographic position of the locations marked by the subject corresponds to the locations detected by the system.

During system testing on route III, as shown in Figure 7b, the passenger marked six discomfort locations. The measuring system detected 22 locations for the same route (Figure 7a). As in previous cases, the cause is the RMS

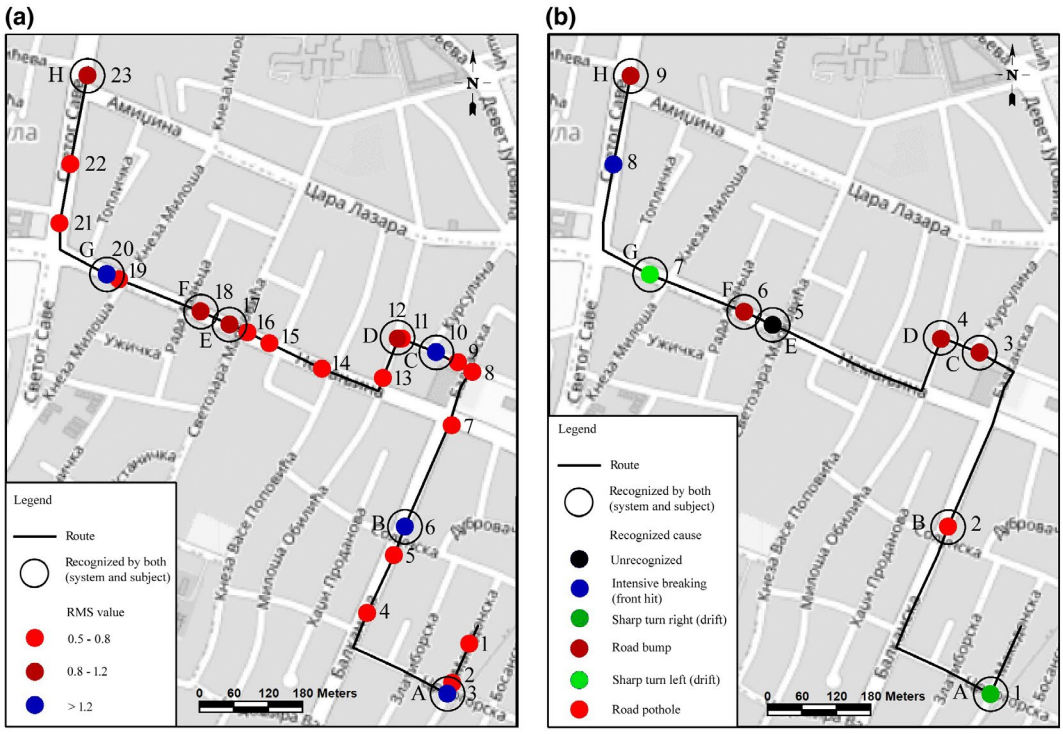

FIGURE 5 Route I. (a) System-detected discomforts with RMS threshold value 0.5G. (b) Discomfort causes marked by a passenger during driving. *Source*: https://www.openstreetmap.org/

threshold value. As in the case of route I, the passenger detected one more location than the system (Table 3). Comparing the markers from both figures, marker no. 5 in Figure 7b (light red) is marked in red on Figure 7a (marker no. 18). Since comfort is a subjective feeling, RMS threshold values could be set lower or higher than the 0.8G used here. As in the previous two cases, all locations marked subjectively by the passengers correspond to those automatically detected by the system.

One of the reasons for the slight differences in the first and third tests may be the age and health condition of the passenger. Unlike the second test, where the passenger was a young and healthy man, in the first test the passenger was a healthy, elderly man, while in the third test the passenger was a younger woman with spinal problems. Regardless of these slight differences during system testing, the measuring system confirmed passengers' comfort calculations in practice.

GIS software was used to analyse the collected comfort values and automatically generate causes of discomfort (DCR). As shown in Figure 3e (with the red circle), a_{peak} is detected and this is the most important value after the one first detected in an insensitive period. It carries information about the discomfort caused. By using the three-axis accelerometer for gathering *X*, *Y*, and *Z* values, the discomfort cause can be determined. The main idea is to calculate the percentage contributions from each axis in the detected a_{peak} and analyse those values in GIS software to determine the cause (type) of the discomfort. This is achieved using the following equations in the GIS:

$$p = \frac{|\text{sample } X| + |\text{sample } Y| + |\text{sample } Z|}{100} \tag{4}$$

$$X_{pr} = \frac{|\text{sample } X|}{p} \tag{5}$$

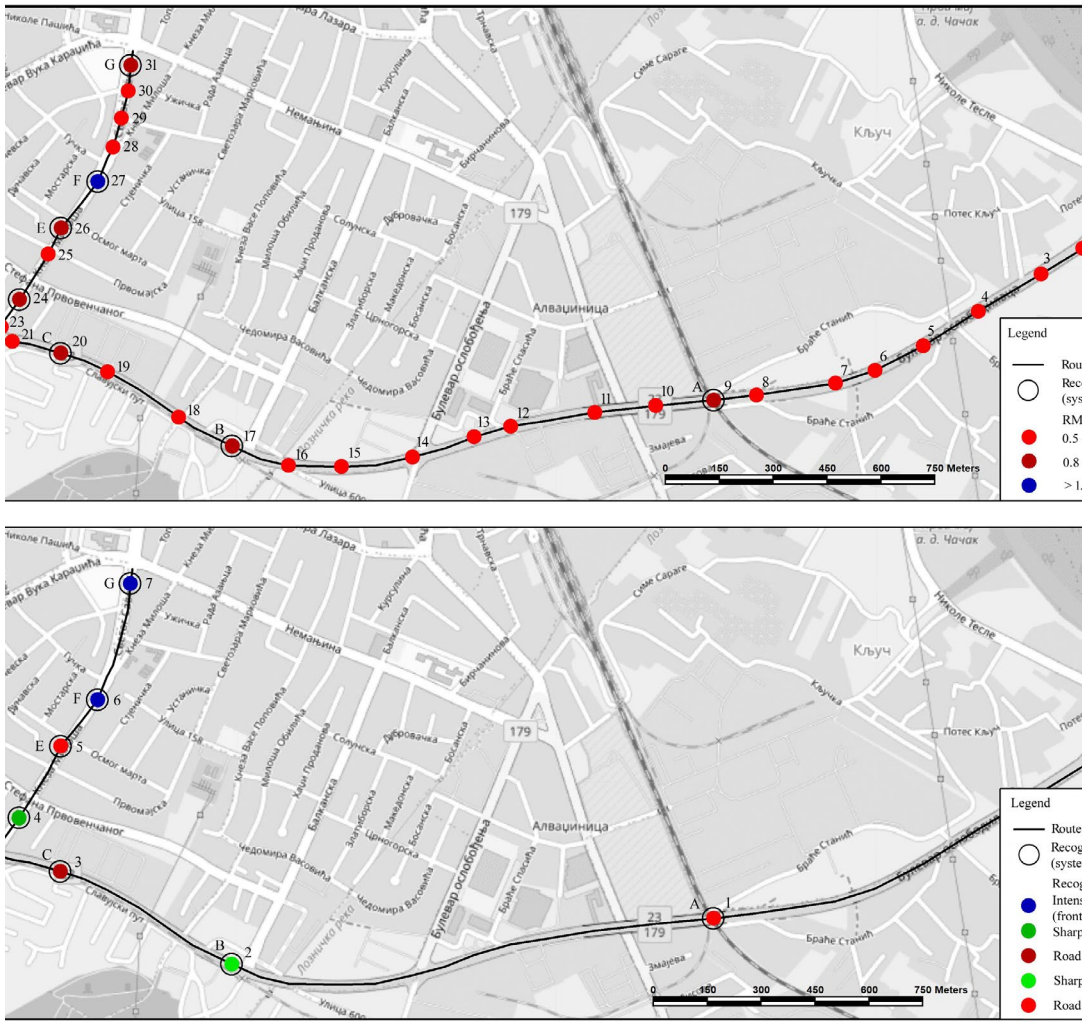

FIGURE 6 Route II. (a) System-detected discomforts with RMS threshold value 0.5G. (b) Discomfort causes marked by a passenger during driving. *Source*: https://www.openstreetmap.org/

$$Y_{pr} = \frac{|\text{sample } Y|}{p} \tag{6}$$

$$Z_{pr} = \frac{|\text{sample } Z|}{p} \tag{7}$$

where p is a percentage absolute axis acceleration sum value and X_{pr}, Y_{pr} and Z_{pr} are axis percentage share values. X_{pr}, Y_{pr} and Z_{pr} sum to 100%. As a result, three percentage values are obtained. All locations detected by the system and marked by passengers with calculated X_{pr}, Y_{pr} and Z_{pr} are shown in Tables 4–6.

The highest percent values which represent the highest axis influence in a_{peak} are shaded grey (Tables 4–6). Discomfort cause types are categorized according to those values and the discomfort categorization shown in Table 2. The system can classify the cause of discomfort if the maximum percentage value exceeds 45%. Otherwise only the location and level of discomfort are detected. This situation is shown in Table 4 as an empty SYSTEM DCR column value. This occurred only once in 20 detected DCRs (5%).

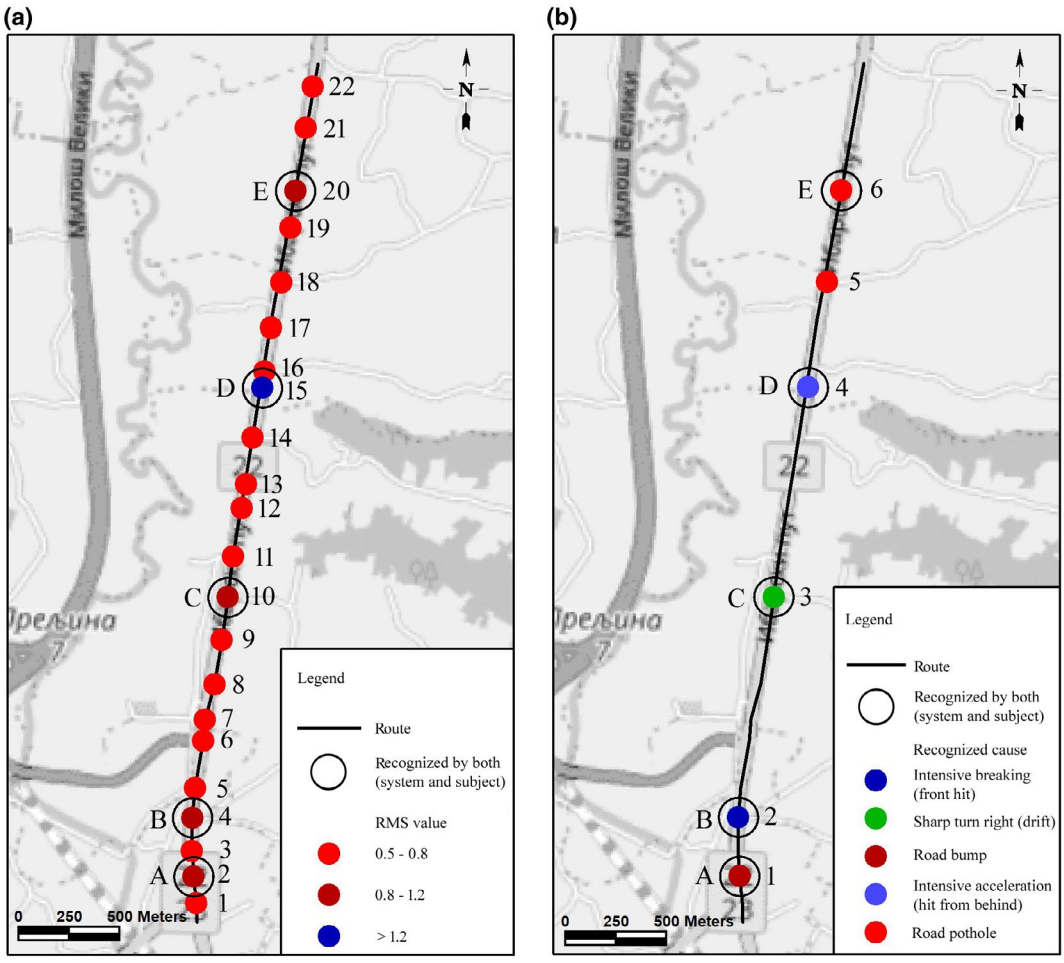

FIGURE 7 Route III. (a) System-detected discomforts with RMS threshold value 0.5G. (b) Discomfort causes marked by a passenger during driving. *Source*: https://www.openstreetmap.org/

TABLE 3 Detected discomforts

Marker	RMS value	Marker count for route I	Marker count for route II	Marker count for route III
Red	0.5–0.8	15	24	17
Dark red	0.8–1.2	4	6	4
Blue	>1.2	4	1	1

4 | CONCLUSIONS

Road surface problems can cause significant vehicle vibrations which are felt by passengers inside the vehicle. These vibrations are the main cause of driving discomfort. Comfort, in particular, is difficult to evaluate objectively, because this is fundamentally subjective, based on the sensitivity of the individual. Thus, the main

TABLE 4 DCR algorithm results for route I

Label	RMS	a_{peak}	X (G)	Y (G)	Z (G)	Velocity	Lat	Lon	Axis X (%)	Axis Y (%)	Axis Z (%)	System_ DCR	Cause recognized by subject
A	1.42	1.87	1.59	0.86	0.48	59.72	43.88062	20.35165	54.10	29.50	16.40	Right	Sharp turn right (Drift)
B	1.55	2.15	0.10	−1.86	1.07	37.22	43.88323	20.35070	3.40	61.30	35.30	Pothole	Road pothole
C	1.47	2.12	0.52	2.06	−0.01	27.50	43.88596	20.35135	20.20	79.50	0.30	Bump	Road bump
D	0.91	1.81	0.48	1.44	0.97	49.14	43.88617	20.35052	16.40	49.90	33.70	Bump	Road bump
E	0.92	1.29	−0.72	0.90	0.57	8.67	43.88637	20.34687	32.90	41.10	26.00		
F	0.86	1.28	0.35	1.02	0.69	40.17	43.88639	20.35157	17.00	49.51	33.49	Bump	Road bump
G	1.72	2.38	−2.30	0.54	−0.28	28.90	43.88714	20.34421	73.60	17.40	9.00	Left	Sharp turn left (Drift)
H	0.90	1.42	0.09	1.41	0.01	55.54	43.89017	20.34432	5.90	93.60	0.50	Bump	Road bump

TABLE 5 DCR algorithm results for route II

Label	RMS	Apeak	*X*-*G*	*Y*-*G*	*Z*-*G*	Velocity	Lat	Lon	Axis *X* %	Axis *Y* %	Axis *Z* %	System_ DCR	Cause recognized by subject
A	0.86	1.64	0.00	−1.52	0.62	59.62	43.87873	20.36315	0.13	71.11	28.76	Pothole	Road pothole
B	0.82	1.48	1.23	−0.03	0.81	57.63	43.87749	20.34657	59.65	1.25	39.10	Left	Sharp turn left (Drift)
C	0.93	1.77	−0.05	1.49	−0.96	62.58	43.87977	20.34065	2.03	59.70	38.27	Bump	Road bump
D	0.95	1.62	1.40	−0.04	0.83	42.80	43.8811	20.33922	61.72	1.67	36.61	Right	Sharp turn right (Drift)
E	0.89	2.11	−0.34	1.49	−1.45	44.15	43.88289	20.34062	10.48	45.36	44.16	Pothole	Road pothole
F	1.34	1.65	0.34	0.28	1.59	40.36	43.88406	20.34188	15.51	12.49	72.00	Break	Intensive breaking (Front hit)
G	0.81	1.82	0.17	−0.24	1.80	26.49	43.88696	20.34298	7.85	10.65	81.50	Break	Intensive breaking (Front hit)

TABLE 6 DCR algorithm results for route III

Label	RMS	Apeak	*X-G*	*Y-G*	*Z-G*	Velocity	Lat	Lon	Axis *X* %	Axis *Y* %	Axis *Z* %	System_DCR	Cause recognized by subject
A	0.87	1.28	−0.31	1.40	−1.18	44.57	43.91315	20.40773	10.66	48.52	40.81	Bump	Road bump
B	0.84	1.49	0.65	−0.51	1.25	63.03	43.91576	20.40763	26.93	21.23	51.84	Break	Intensive breaking (Front hit)
C	0.87	1.25	1.16	−0.41	−0.17	68.72	43.92553	20.4097	66.74	23.44	9.82	Right	Sharp turn right (Drift)
D	1.29	2.37	−0.14	0.15	−2.36	71.35	43.93482	20.41173	5.40	5.69	88.91	Acceleration	Intensive acceleration (Hit from behind)
E	0.82	1.61	−0.76	−1.24	0.40	86.90	43.94356	20.41367	31.55	51.61	16.84	Pothole	Road pothole

aim of this article was the automation of a discomfort cause recognition process without human activity. One of the main problems in such work was defining appropriate comfort threshold value-system sensitivity, since lower values produce more locations while higher values detect only high discomfort causes. The low-resource algorithm presented in this article is developed and tested within a GIS. The novelty in this article is the use of a GIS to automate the process of discomfort cause recognition and the possibility of visualization of the obtained locations. Calculated values can be integrated into the measuring system with automatic discomfort cause recognition.

Although the tests showed a high degree of correlation between the results, further research should be undertaken in different weather conditions and different geographical locations with passengers of different physical-psychological profiles, to fully confirm its applicability.

The system presented and tested would be of great importance for the transport of patients because their health conditions usually require the most comfortable driving experience. However, this system could also be very useful to highways agencies for cost-effective detection of road conditions for road maintenance since the type of road discomfort cause is detected. Also, vehicles could be compared by comfort value or by the number of detected discomforts caused while driving on the same road. Live data transmission is also possible. This would allow live road problem detection and road surface problems. As a result of prolonged usage of the system, road comfort quality maps with discomfort types could be created. Drivers could determine paths with the least discomfort to their destinations.

ACKNOWLEDGMENTS

Work presented in this article was supported by Intergraph RRI Lab at FTN Cacak with Intergaph and Intergraph Partner GIS Solutions. Also, part of this work is included in a projects No. 176008, No. 176017 and No 451-03-9/2021-14/200132, financed by the Ministry of Education, Science and Technological Development of the Republic of Serbia.

CONFLICT OF INTEREST

The authors of this manuscript have no conflict of interest to declare.

DATA AVAILABILITY STATEMENT

Research data are not shared.

ORCID

Aleksandar Peulić https://orcid.org/0000-0003-3043-6879
Miodrag Peulić https://orcid.org/0000-0002-5984-2902
Sanja Stojković https://orcid.org/0000-0003-2292-5082
Nemanja Vagić https://orcid.org/0000-0002-8639-0585

REFERENCES

Battié, M. C., Videman, T., Gibbons, L. E., Manninen, H., Gill, K., Pope, M., & Kaprio, J. (2002). Occupational driving and lumbar disc degeneration: A case control study. *The Lancet*, *360*(9343), 1369–1374. https://doi.org/10.1016/S0140-6736(02)11399-7

British Standards Institution. (1987). *Measurement and evaluation of human exposure to whole-body mechanical vibration and repeated shock* (BS 6841: 1987). London, UK: BSI.

Cleon, L. M., & Laurkis, G. (1996). Evaluation of passenger comfort in railway vehicles. *Journal of Low Frequency Noise and Vibration*, *15*(2), 53–69. https://doi.org/10.1177/026309239601500201

Cuadrado, J., Dopico, D., Perez, J. A., & Pastorino, R. (2012). Automotive observers based on multibody models and the extended Kalman filter. *Multibody Systems Dynamics*, *27*(1), 3–19. https://doi.org/10.1007/s11044-011-9251-1

Eriksson, J., Girod, L., Hull, B., Newton, R., Madden, S., & Balakrishnan, H. (2008). The Pothole Patrol: Using a mobile sensor network for road surface monitoring. *In Proceedings of the Sixth International Conference on Mobile Systems, Applications, and Services, Breckenridge, CO* (pp. 29–39). New York, NY: ACM. https://doi.org/10.1145/1378600.1378605

Fenchea, M., & Boltosi, A. (2006). Influence of suspension on the vehicle dynamic performance. *Annals of the University of Oradea, Fascicle of Management and Technological Engineering*, *5*(15), 373–378.

Gray, A., Bush, S., & Whiteley, S. (2004). Secondary transport of the critically ill and injured adult. *Emergency Medicine Journal*, *21*, 281–285. https://doi.org/10.1136/emj.2003.005975

Gruevski, K. M., Holmes, M. W. R., Gooyers, C. E., Dickerson, C. R., & Callaghan, J. P. (2016). Lumbar postures, seat interface pressures and discomfort responses to a novel thoracic support for police officers during prolonged simulated driving exposures. *Applied Ergonomics*, *52*, 160–168. https://doi.org/10.1016/j.apergo.2015.07.015

GUP. (2019). Grada Čačka. Retrieved from http://212.200.27.238/gupCacak/

International Organization for Standardization. (1997). *Mechanical vibration and shock: Evaluation of human exposure to whole-body vibration. Part 1: General requirements* (ISO 2631-1). Geneva, Switzerland: Author.

Jianmin, S., & Qingmei, Y. (2009). Advanced suspension systems for improving vehicle comfort. In *Proceedings of the 2009 IEEE International Conference on Automation and Logistics, Shenyang, China* (pp. 1264–1267). Piscataway, NJ: IEEE. https://doi.org/10.1109/ICAL.2009.5262768

Jovanović, Ž., Blagojević, M., Janković, D., & Peulić, A. (2019). Patient comfort level prediction during transport using artificial neural network. *Turkish Journal of Electrical Engineering and Computer Sciences*, *27*, 2817–2832. https://doi.org/10.3906/elk-1807-258

Junoh, A. K., Wan Muhamad, W. Z. A., Nopiah, Z., Mohd Nor, J., Ariffin, A. K., & Fouladi, M. (2011). A study on the effects of tyre to vehicle acoustical comfort in passenger car cabin. In *Proceedings of the Third International Conference on Computer Research and Development, Shanghai, China* (Vol. *4*, pp. 342–345). Piscataway, NJ: IEEE. https://doi.org/10.1109/ICCRD.2011.5763889

Lee, K., & Kwan, M. P. (2018). Automatic physical activity and in-vehicle status classification based on GPS and accelerometer data: A hierarchical classification approach using machine learning techniques. *Transactions in GIS*, *22*, 1522–1549. https://doi.org/10.1111/tgis.12485

Li, X., Goldberg, D. W., Chu, T., & Ma, A. (2019). Enhancing driving safety: Discovering individualized hazardous driving scenes using GIS and mobile sensing. *Transactions in GIS*, *23*, 538–557. https://doi.org/10.1111/tgis.12540

Mohan, P., Padmanabhan, V. N., & Ramjee, R. (2008). Nericell: Rich monitoring of road and traffic conditions using mobile smartphones. In *Proceedings of the Sixth ACM Conference on Embedded Networked Sensor Systems, Raleigh, NC* (pp. 323–336). New York, NY: ACM. https://doi.org/10.1145/1460412.1460444

Oijer, F., & Edlund, S. (2003). Complete vehicle durability assessments using discrete sets of random roads and transient obstacles based on Q-distributions. *Vehicle System Dynamics*, *37*, 67–74. https://doi.org/10.1080/00423114.2002.11666221

Oijer, F., & Edlund, S. (2004). Identification of transient road obstacle distributions and their impact on vehicle durability and driver comfort. *Vehicle System Dynamics*, *41*, 744–753.

Open Geospatial Consortium. (2015). *OGC KML 2.3*. Retrieved from http://www.opengis.net/doc/IS/kml/2.3

Paulraj, M. P., Yaacob, S., & Andrew, A. M. (2010). Vehicle noise comfort level indication: A psychoacoustic approach. In *Proceedings of the Sixth International Signal Processing and Its Applications Colloquium*. Melaka, Malaysia (pp. 73-77). Piscataway, NJ: IEEE. https://doi.org/10.1109/CSPA.2010.5545249

Schmidt, C., & Diedrich, C. (2007). Specification of test rules for vehicle comfort systems with formalized models and methods. In *Proceedings of the Fourth IEEE International Conference onIndustrial Informatics, Singapore* (pp. 1118–1123). Piscataway, NJ: IEEE. https://doi.org/10.1109/INDIN.2006.275774

Strahman, J., Dueker, K., & Kimpel, T. (2000). Service reliability impacts of computer-aided dispatching and automatic vehicle location technology: A tri-met case study. *Transportation Quarterly*, *54*(3), 85–102.

Tan, C., & Park, S. (2005). Design of accelerometer-based inertial navigation systems. *IEEE Transactions on Instrumentation and Measurement*, *54*(6), 2520–2530. https://doi.org/10.1109/TIM.2005.858129

Wang, Q., Qian, L., Tang, Y., Wen, Q., & Chen, W. (2000). Research on the suspension CAD of farm transport vehicle based on ride comfort simulation. *Transactions of the Chinese Society of Agricultural Machinery*, *31*(6), 25–27.

Wheble, V. H. (1987). Ambulance transport: A question of patient comfort. *Engineering in Medicine*, *16*(1), 47–50. https://doi.org/10.1243/emed_jour_1987_016_011_02

Wu, Z. H., Wu, Q., Chen, H., Pan, G., Zhao, M., & Sun, J. (2007). ScudWare: A semantic and adaptive middleware platform for smart vehicle space. *IEEE Transactions on Intelligent Transportation Systems*, *8*(1), 121–132. https://doi.org/10.1109/TITS.2006.890080

Xiandong, L., Zhidang, D., & Feng, G. (2003). Research on the method of simulating road roughness numerically. *Journal of Beijing University of Aeronautics and Astronautics*, *29*(9), 843–846.

Yangi, X. (2007). Development of simulation models of vehicle riding comfort. *Journal of Nanjing Institute of Technology (Natural Science Edition)*, *3*, 66–70.

Zhang, X. Y. (2018). Study on ride comfort of the articulated dump truck. *In Proceedings of the Fifth International Conference on Information Science and Control Engineering, Zhengzhou, China* (pp. 527–532). Piscataway, NJ: IEEE. https://doi.org/10.1109/ICISCE.2018.00116

Zhao, D., & Stefanakis, E. (2018). Integrated compression of vehicle spatio-temporal trajectories under the road stroke network constraint. *Transactions in GIS*, *22*, 991–1007. https://doi.org/10.1111/tgis.12464

How to cite this article: Peulić, A., Peulić, M., Jovanović, Ž., Joković, M., Stojković, S., & Vagić, N. (2021). Locating and categorizing causes of discomfort during transport of patients to medical facilities. *Transactions in GIS*, 25, 2963–2981. https://doi.org/10.1111/tgis.12797